



Article

Highly Efficient Capture of Volatile Iodine by Conjugated Microporous Polymers Constructed Using Planar 3- and 4-Connected Organic Monomers

Chaohui Li ^{1,†}, Qianqian Yan ^{1,†}, Huanjun Xu ², Siyu Luo ¹ , Hui Hu ^{1,*}, Shenglin Wang ^{1,*}, Xiaofang Su ¹, Songtao Xiao ³ and Yanan Gao ¹ 

¹ Key Laboratory of Ministry of Education for Advanced Materials in Tropical Island Resources, Hainan University, No 58, Renmin Avenue, Haikou 570228, China; lich@hainanu.edu.cn (C.L.); yanqianqian@hainanu.edu.cn (Q.Y.); 2021220856000114@hainanu.edu.cn (S.L.); sxf@hainanu.edu.cn (X.S.); ygao@hainanu.edu.cn (Y.G.)

² School of Science, Qiongtai Normal University, Haikou 571127, China; xuhuanjun86@iccas.ac.cn

³ China Institute of Atomic Energy, Beijing 102413, China; xiao200112@163.com

* Correspondence: hhu@hainanu.edu.cn (H.H.); wangshenglin@hainanu.edu.cn (S.W.)

† These authors contributed equally to this work.

Abstract: The effective capture and recovery of radioiodine species associated with nuclear fuel reprocessing is of significant importance in nuclear power plants. Porous materials have been proven to be one of the most effective adsorbents for the capture of radioiodine. In this work, we design and synthesize a series of conjugated microporous polymers (CMPs), namely, TPDA–TFPB CMP, TPDA–TATBA CMP, and TPDA–TECHO CMP, which are constructed based on a planar rectangular 4-connected organic monomer and three triangular 3-connected organic monomers, respectively. The resultant CMPs are characterized using various characterization techniques and used as effective adsorbents for iodine capture. Our experiments indicated that the CMPs exhibit excellent iodine adsorption capacities as high as 6.48, 6.25, and 6.37 g g^{−1} at 348 K and ambient pressure. The adsorption mechanism was further investigated and the strong chemical adsorption between the iodine and the imine/tertiary ammonia of the CMPs, 3D network structure with accessible hierarchical pores, uniform micromorphology, wide π -conjugated structure, and high-density Lewis-base sites synergistically contribute to their excellent iodine adsorption performance. Moreover, the CMPs demonstrated good recyclability. This work provides guidance for the construction of novel iodine adsorbent materials with high efficiency in the nuclear power field.

Keywords: conjugated microporous polymers; topology; iodine adsorption; porous materials; nuclear energy



Citation: Li, C.; Yan, Q.; Xu, H.; Luo, S.; Hu, H.; Wang, S.; Su, X.; Xiao, S.; Gao, Y. Highly Efficient Capture of Volatile Iodine by Conjugated Microporous Polymers Constructed Using Planar 3- and 4-Connected Organic Monomers. *Molecules* **2024**, *29*, 2242. <https://doi.org/10.3390/molecules29102242>

Academic Editor: Xinhua Qi

Received: 29 March 2024

Revised: 2 May 2024

Accepted: 5 May 2024

Published: 10 May 2024



Copyright: © 2024 by the authors. Licensee MDPI, Basel, Switzerland. This article is an open access article distributed under the terms and conditions of the Creative Commons Attribution (CC BY) license (<https://creativecommons.org/licenses/by/4.0/>).

1. Introduction

Over the past few decades, nuclear power has come to be considered one of the most important sources of green and clean energy in the world [1,2]. However, the safe disposal and proper management of radioactive waste generated from the spent nuclear fuel remain a great challenge. Among various nuclear wastes, radionuclide ¹²⁹I (15.7-million-year half-life) and ¹³¹I have been identified as the two most significant volatile waste species, as their quick diffusion into air and environment would cause radiological contamination in terms of both the global environment and biological health [3–5]. In fact, an increased incidence of thyroid cancer was observed following the Chernobyl and Mayak accidents [6]. Therefore, the development of novel materials to effectively dispose of these nuclear wastes has become an extremely important and urgent task.

By far, adsorption is regarded as an effective strategy for radioiodine removal due to advantages such as easy operation, high efficiency, low cost, and so on. In recent

years, various adsorbent materials have been developed for iodine capture, including inorganic zeolites [7,8], activated carbon [9,10], and silver-doped mordenite [11], as well as organic–inorganic hybrid materials (mainly referring to metal–organic frameworks, MOFs [12–15]), and organic porous framework materials such as covalent organic frameworks (COFs) [16–20], conjugated microporous polymers (CMPs) [21–24], porous aromatic frameworks (PAFs) [25–27], porous organic frameworks (POFs) [28], hyper crosslinked polymers (HCPs) [29,30], etc. Among them, organic porous framework materials appear to be one of the most effective adsorbents for iodine capture [5].

As a special class of organic porous frameworks, CMPs, combine extended π -conjugated structures with permanent micropores and have attracted much attention due to their unique electronic properties, structural modularity, high porosity, and good thermal and chemical stability [31]. Organic monomers with three or more cross-linking sites and rigid structures are needed to construct CMPs. The monomers are connected through covalent bonds and the networks extend along a three-dimensional (3D) direction, leaving voids between the rigid monomers, and thus giving CMPs porosity [32]. As a result, CMPs allow access for guest molecules to “touch” all the atoms of the skeleton. Therefore, CMPs represent an ideal platform for adsorbent materials. Moreover, the porosity of CMPs can be regulated by changing the size and geometric shape of the rigid monomers [33]. In other words, the desired structures of CMPs can be achieved through topology-directed design. This topology-directed strategy has been successfully applied to a series of PAFs to obtain low-crystalline or amorphous frameworks [32–37]. In some cases, preferential topological structures with regular pores have been achieved [38–40]. Therefore, the rational design of organic monomers under the guidance of topology chemistry enables organic porous frameworks to give predesigned structure and functionality. The symmetry of organic monomers affects pore structure and dimension, which are known to be determinative of the properties of materials [32]. Take iodine adsorption as an example, tuning pore sizes and pore structures of organic porous frameworks was found to play important roles in iodine uptake capacity [41–45].

Herein, we design and synthesize a series of new CMPs that were readily obtained through the condensation of a planar rectangular 4-connected N1,N1'-(1,4-phenylene)bis(N1-(4-aminophenyl)benzene-1,4-diamine) (TPDA) and triangular 3-connected 1,3,5-tris(4-formylphenyl)benzene (TFPB), 4,4',4''-(1,3,5-triazine-2,4,6-triyl)tris[benzaldehyde] (TATBA), and 4,4',4''-(1,3,5-benzenetriyl)tri-2,1-ethynediyl)tris[benzaldehyde] (TECHO) organic monomers, respectively (Figure 1). The combination of 4-connected and 3-connected monomers could present a preferential 3D network (see possible topological structures in Figure S1) although only amorphous structures of the CMPs are obtained in this work. The resultant TPDA–TFPB CMP, TPDA–TATBA CMP, and TPDA–TECHO CMP have moderate special surface areas (ranging from 262 to 426 m² g^{−1}) but show excellent volatile iodine adsorption capacities as high as 6.48, 6.25, and 6.37 g g^{−1}, respectively. We consider that such high iodine adsorption capacities of the CMPs could be ascribed to their 3D topological structures, hierarchical pores, π -conjugated structure, uniform micromorphology, and high-density Lewis-base sites. In addition, the captured iodine within the porosities of CMPs can be rapidly released into methanol and the CMPs can be recycled many times without obvious loss in adsorption capability.

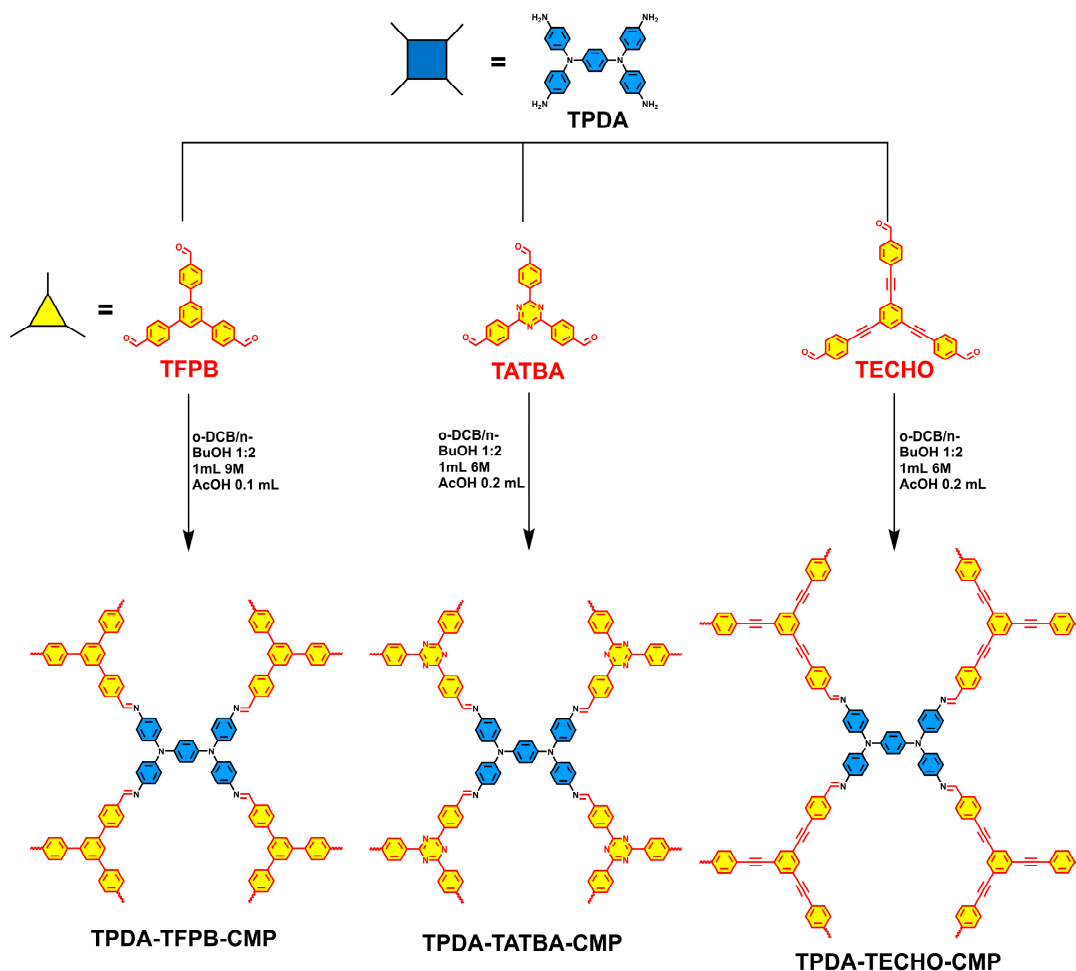


Figure 1. Synthesis routes for TPDA–TFPB CMP, TPDA–TATBA CMP, and TPDA–TECHO CMP.

2. Results and Discussion

Synthesis and characterization. The synthesis routes of the three CMPs, termed TPDA–TFPB CMP, TPDA–TATBA CMP, and TPDA–TECHO CMP, are shown in Figure 1. The synthesis details of the organic monomers and their corresponding ^1H NMR spectra (Figures S2 and S3) [46,47] are given in supporting information (SI). The formation of the CMPs can be demonstrated by FT-IR spectra (Figure 2). It is clear that after condensation reactions, the stretching bands of $-\text{NH}_2$ in TPDA at 3446 and 3352 cm^{-1} and the aldehyde stretching bands of 3-connected aromatic aldehydes (1680 cm^{-1} for TFPB; 1691 cm^{-1} for TATBA and TECHO) were remarkably decreased. Meanwhile, new peaks were observed (1610 cm^{-1} for TPDA–TFPB CMP, 1618 cm^{-1} for TPDA–TATBA CMP, and 1605 cm^{-1} for TPDA–TECHO CMP), which can be ascribed to the formation of imine groups. This reveals that the three CMPs were constructed through imine linkage. Note that the new peak of imine was superimposable on the signals of residual aldehyde groups, suggesting an incomplete condensation reaction. For this reason, the formation of imine linkages needs to be confirmed by solid-state ^{13}C CP/MAS NMR spectroscopy (Figure S4). The peaks around $150\text{--}160\text{ ppm}$ can be attributed to the carbon atom of the imine linkages, while the peaks around $190\text{--}195\text{ ppm}$ can be assigned to the unreacted aldehyde groups. The incomplete condensation may be due to the highly branched connection of 4-connected and 3-connected monomers. It is also worth noting that the discrepancies between theoretical and experimental values in element analysis were observed in all POPs. The possible reason, we think, could be due to the organic residues that are not completely removed during the purification process or insufficient drying treatment that retains some organic solvents.

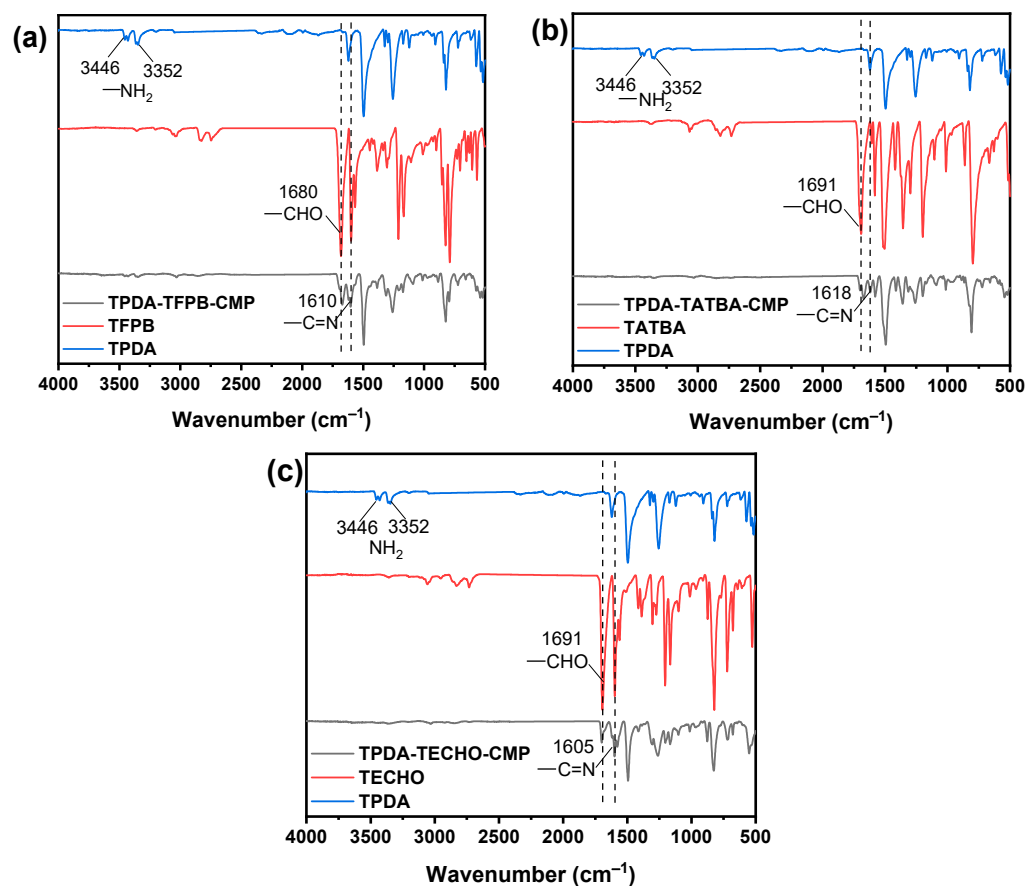


Figure 2. FT-IR spectra of TFPB, TPDA, and TPDA-TFPB CMP (a), TATBA, TPDA, and TPDA-TATBA CMP (b), and TECHO, TPDA, and TPDA-TECHO CMP (c).

The porosity of the CMPs was characterized by nitrogen adsorption isotherm measurements at 77 K. It can be seen from Figure 3 that the CMPs exhibited combined Type I/IV sorption curves, suggesting the presence of micropores and mesopores. The N_2 adsorption capacity of the CMPs increases sharply when the relative pressure, P/P_0 , is less than 0.1, indicating the existence of a large number of micropores in the three CMPs. When the P/P_0 ranges from 0.1 to 0.9, their N_2 adsorption capacity increases slowly, with a hysteresis loop observed in the adsorption–desorption isotherms, which suggests the presence of mesoporous structures in the CMPs. Additionally, when the P/P_0 is in the range of 0.9 to 1.0, the N_2 adsorption capabilities of TPDA-TFPB CMP, TPDA-TATBA CMP, and TPDA-TECHO CMP increase sharply again, indicating the coexistence of macropores in the three CMPs. The Brunauer–Emmett–Teller (BET) surface areas of TPDA-TFPB CMP, TPDA-TATBA CMP, and TPDA-TECHO CMP were calculated to be 284, 427, and 262 $\text{m}^2 \text{g}^{-1}$, and the corresponding pore volumes were estimated to be 0.26, 0.28, and 0.22 $\text{cm}^3 \text{g}^{-1}$, respectively. Based on the NLDFT, the average pore diameters of the three CMPs were estimated to be 2.5, 2.1, and 3.3 nm, respectively, revealing that the CMPs are mainly determined by their microporous structures.

The thermostability of the CMPs was investigated using TGA measurements (Figure S5). The three CMPs exhibited high decomposition temperatures of over 480 $^\circ\text{C}$, revealing their good thermal stability. The micromorphology of the CMPs was characterized by FE-SEM observation. It is evident from Figure 4 that the CMPs are all composed of clusters of irregular particles. These particles are uniformly stacked, which is favorable for gas adsorption.

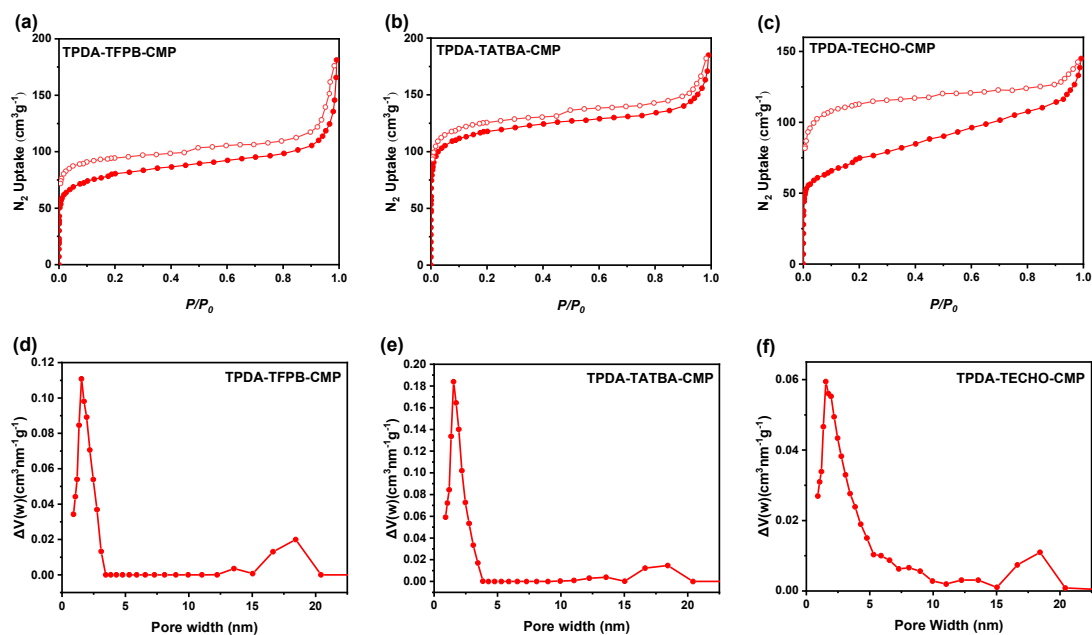


Figure 3. N_2 adsorption and desorption isotherms of TPDA-TFPB CMP (a), TPDA-TATBA CMP (b), and TPDA-TECHO CMP (c), and their corresponding pore size distributions (d–f).

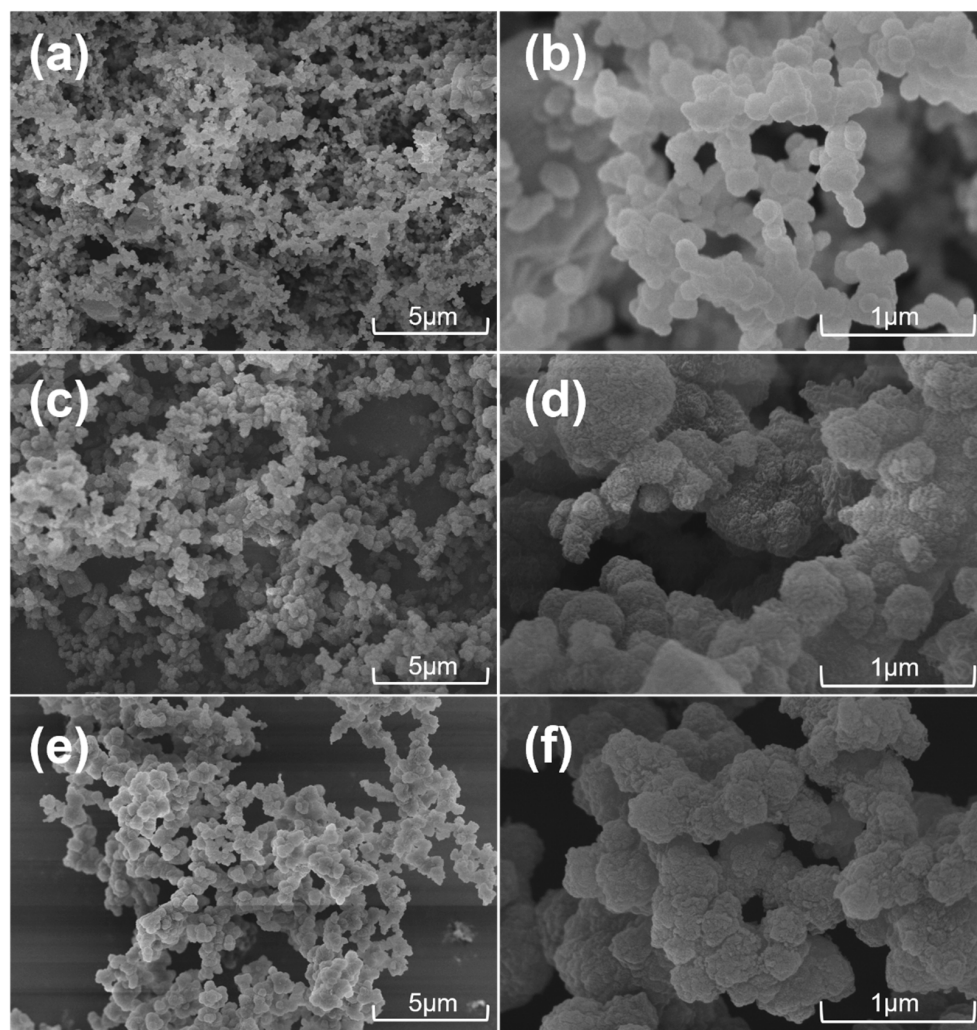


Figure 4. The FE-SEM images of TPDA-TFPB CMP (a,b), TPDA-TATBA CMP (c,d), and TPDA-TECHO CMP (e,f), as shown at different scale sizes.

Iodine vapor capture by CMPs. Because of their uniform morphologies, high porosities, good thermostability, and 3D networks with π -conjugated structures, the CMPs can be good candidates for iodine vapor adsorption. The gravimetric method was used to investigate the volatile iodine capture capacity of CMPs as described in a previous report [16,21]. A certain amount of CMP adsorbent and excess iodine were separated and put in a closed bottle at 348 K and under ambient pressure. The changes in the weight of the CMP adsorbent were recorded over time, and thus the iodine adsorption capacity of the CMP at different time intervals was calculated (see details in the SI). The iodine vapor adsorption behaviors of the CMPs over time are shown in Figure 5. It is evident that iodine vapor can be quickly adsorbed in a short time, suggesting fast adsorption behavior and good adsorption capability. The hierarchical porous structures of the CMPs may lead to their fast adsorption behavior. The adsorption capability of the CMPs increased over time and reached the saturated adsorption capacity after about 60 h. The color of the CMP samples became deep/dark (Figure S6), suggesting a high degree of I_2 adsorption. The saturated adsorption capacity of TPDA-TFPB CMP, TPDA-TATBA CMP, and TPDA-TECHO CMP was 6.48, 6.25, and 6.37 g g⁻¹, respectively, demonstrating their excellent iodine adsorption capacities. Note that these values are higher than those in most of the reported materials (Table S1) [3,5,7,13,16–18,21,24,28,42,46–87].

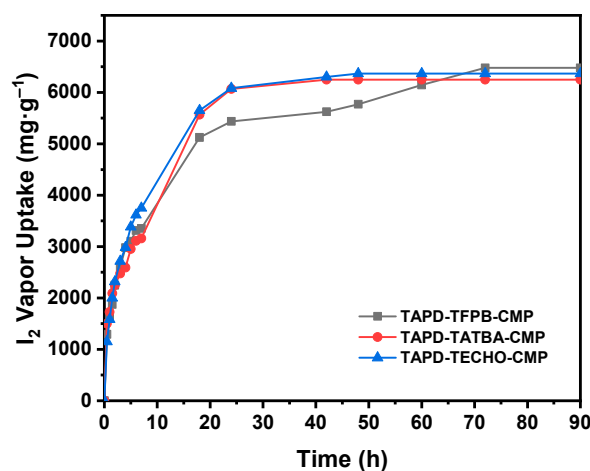


Figure 5. Iodine vapor adsorption curves of TPDA-TFPB CMP, TPDA-TATBA CMP, and TPDA-TECHO CMP at 348 K under ambient pressure.

The 4-connected and 3-connected building units are both planar π -conjugated molecular structures; however, the combination of 4-connected and 3-connected building units produces 3D extended networks [88,89]. Despite the amorphous structure of the CMPs obtained in this work (Figure S7), it can be predicted that their networks will grow preferentially along the predesigned topological structure to the present 3D skeletons. Actually, some PAFs constructed by irreversible covalent bonds have shown low crystalline structures with ordered porosity [34–37]. Therefore, we believe that the 3D extended networks with the accessible π -conjugated structure of the CMPs could lead to their ultrahigh iodine adsorption capacity. In addition, the high density of electron-donating imine linkages throughout the skeletons of CMPs also contributes to their adsorption capacity [16,21]. After I_2 saturation adsorption, no diffraction peaks attributable to I_2 crystals were observed in all I_2 ⊃CMPs (Figure S7), suggesting that no crystalline iodine was deposited on the surface of CMPs. The retention capacity of iodine is also an important parameter for characterizing iodine adsorbent performance. As shown in Figure S5, the iodine-loaded CMPs (designated as I_2 ⊃CMP) showed a mass loss of iodine at about 100 °C, revealing their good retention capacities. The I_2 adsorption capabilities of the CMPs in n-hexane solvent were also investigated using UV-vis spectra (Figures S8 and S9). The adsorption capabilities of TPDA-TFPB CMP, TPDA-TATBA CMP, and TPDA-TECHO CMP were 200, 157, and

160 mg g^{−1}, respectively, when the concentration of I₂ in n-hexane was 100 mg L^{−1}. Their corresponding adsorption capabilities were 542, 547, and 488 mg g^{−1} when the concentration of I₂ in n-hexane was 300 mg L^{−1}, and 874, 850, and 784 mg g^{−1} when the concentration of I₂ in n-hexane was 500 mg L^{−1}. Clearly, the CMPs also exhibited good I₂ adsorption capabilities in n-hexane.

Behavior of iodine release from CMPs and their recyclability. The behavior of iodine release from CMPs was also investigated. Iodine release into methanol was monitored by UV–vis adsorption spectroscopy at room temperature (Figure S10). Figure 6 shows the behavior of iodine release from the iodine-saturated CMPs. It can be seen that the release ratio of the CMPs can reach 80 wt%, although TPDA–TFPB CMP demonstrated a release ratio of nearly 100 wt%. The release curves were fitted using Origin software version 10.1 (The simulated equations are inserted in Figure 6). It can be seen that the concentration of iodine released into methanol increased exponentially with time, suggesting an ultrafast release capability of the CMPs, which is different from the MOFs that released iodine into a solvent in a linear fashion [50,51]. However, the release rates of the I₂-loaded CMPs (I₂≅CMPs) are slower than those of 2D or 3D COFs [16,43]. The reason is that COFs have ordered one-dimensional (1D) open channel structures favoring the ultrarapid release of iodine molecules. The recyclability of the CMPs was also investigated (Figure S11). The iodine adsorbed by I₂≅TPDA–TFPB CMP, I₂≅TPDA–TATBA CMP, and I₂≅TPDA–TECHO CMP was completely removed into methanol by Soxhlet extraction, and the empty CMPs were dried and then reused to capture iodine vapor. The same procedure was repeated several times. It is evident that the iodine adsorption capabilities of the three CMPs decreased slightly after five cycles; however, more than 80% adsorption capacity was still maintained, suggesting their good recyclability.

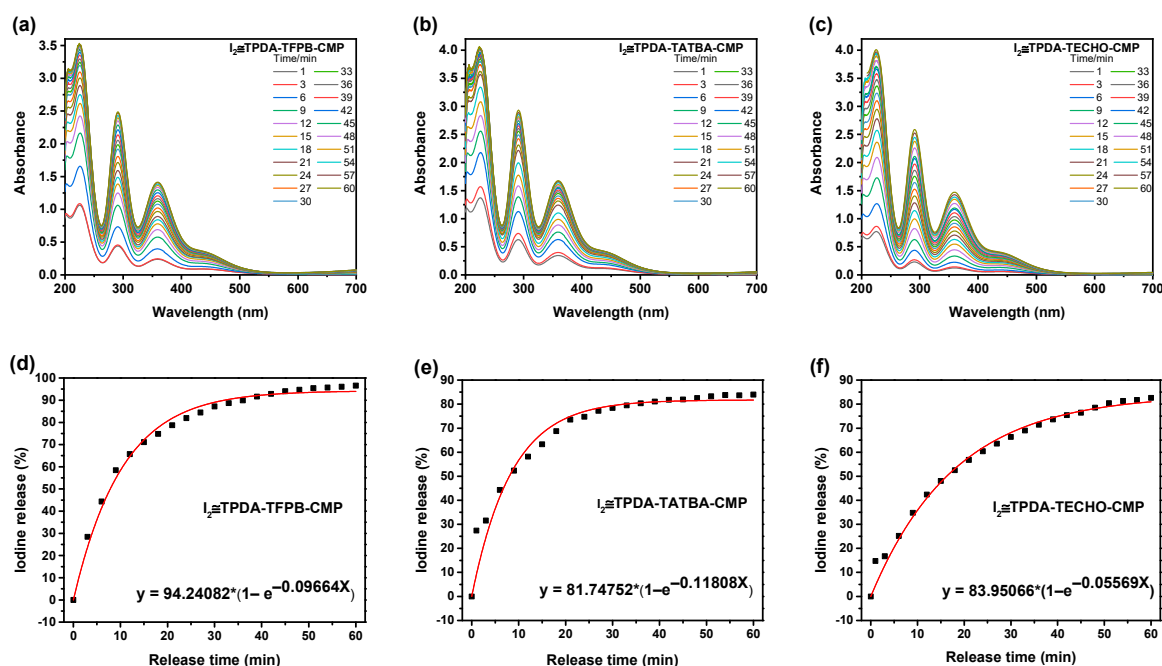


Figure 6. The behavior of iodine release from the I₂≅TPDA–TFPB CMP (a,d), I₂≅TPDA–TATBA CMP (b,e), and I₂≅TPDA–TECHO CMP (c,f) into methanol with time.

Investigation of adsorption mechanism. To analyze the interaction between the adsorbed iodine and the skeleton of the CMPs, FT-IR measurements were used to investigate the effect of iodine on the FT-IR spectrum (Figure 7). It is clear that the FT-IR spectrum changed with adsorption time. Take TPDA–TFPB CMP as an example; the stretching vibration of the imine linkages at 1610 cm^{−1} shifted to 1580 cm^{−1} in the first 10 min, suggesting that there are strong interactions between the iodine and the imine groups. The Lewis-base

imines are the preferred adsorption sites because of the Lewis-acidic nature of iodine [16]. This peak of the imine disappeared gradually, and a new peak concomitantly appeared with adsorption time, which indicates that the iodine was chemically adsorbed by the imine linkages and charge transfer complexes formed between the iodine and the imine linkages [44]. Likewise, these changes were also observed in the stretching vibration of -C-N- of tertiary ammonia at 1200 cm^{-1} in the TPDA group of the CMPs, suggesting that the tertiary ammonia groups are also strong chemical adsorption sites for iodine. These changes in imine and tertiary ammonia groups were also observed in TPDA-TATBA CMP and TPDA-TECHO CMP. The strong chemical adsorption can be considered the main reason that the CMPs exhibited ultrahigh iodine adsorption capabilities. In addition, the 3D network structures with accessible hierarchical pores, uniform micromorphology, and high-density Lewis-base imine linkages of the CMPs may synergistically contribute to their excellent iodine adsorption performance.

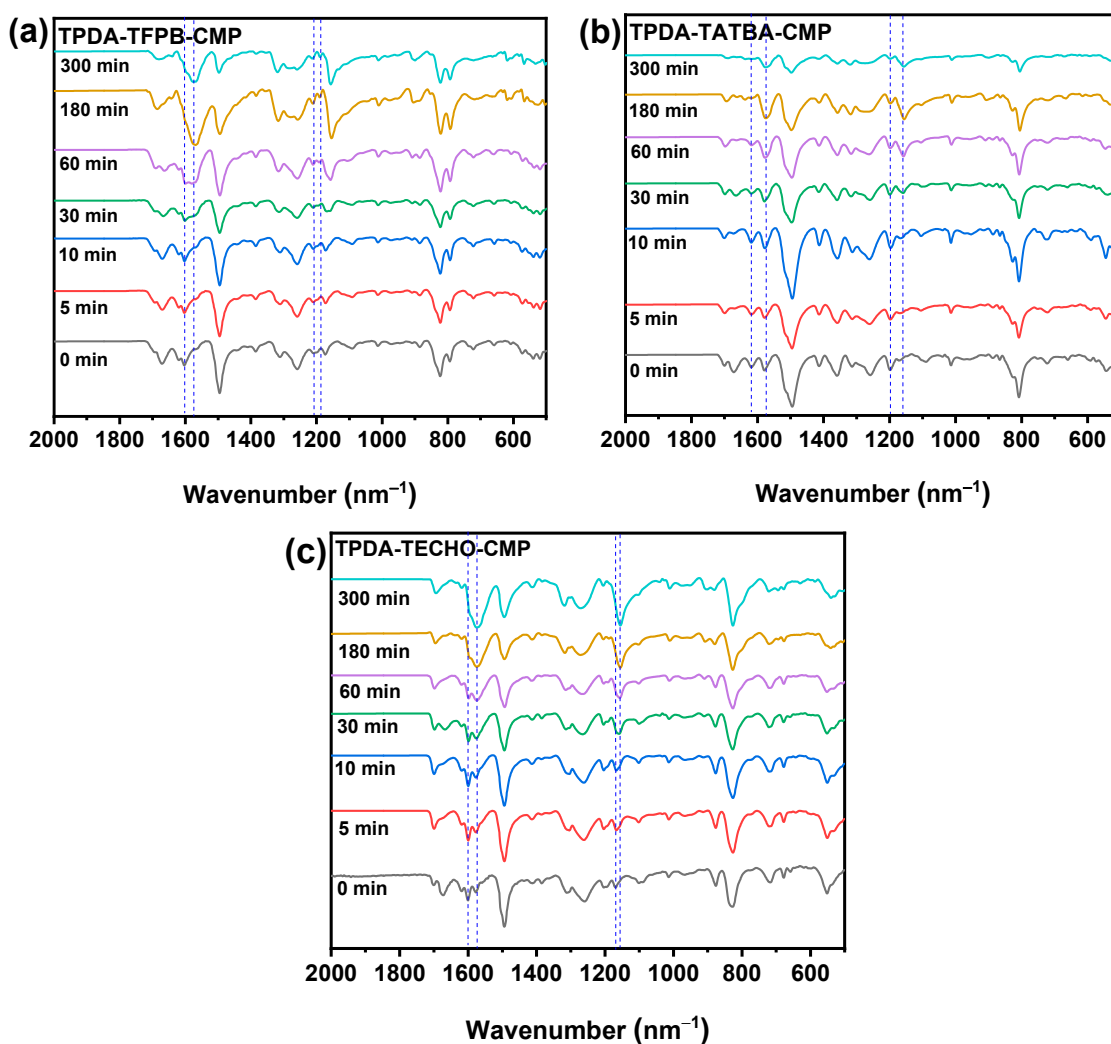


Figure 7. Effect of adsorbed iodine on the FT-IR spectra of TPDA-TFPB-CMP (a), TPDA-TATBA-CMP (b), and TPDA-TECHO-CMP (c).

The Raman spectrum is another powerful tool for characterizing the formation of polyiodide anions. After the adsorption of iodine, two clear bands, at 167 and 112 cm^{-1} , for $\text{I}_2 \cong \text{TPDA-TFPB CMP}$ and $\text{I}_2 \cong \text{TPDA-TATBA CMP}$, and at 169 and 113 cm^{-1} for $\text{I}_2 \cong \text{TPDA-TECHO CMP}$ were observed (Figure 8). The bands at low wavenumbers (112 and 113 cm^{-1}) are due to the symmetric stretching vibration of I_3^- ions, and the bands at high wavenumbers (167 and 169 cm^{-1}) are associated with the stretching vibration of

polyiodide I_5^- [16,21,53]. These results confirm the formation of charge transfer complexes between the captured iodine and the imines, as well as the tertiary ammonia groups of the CMPs.

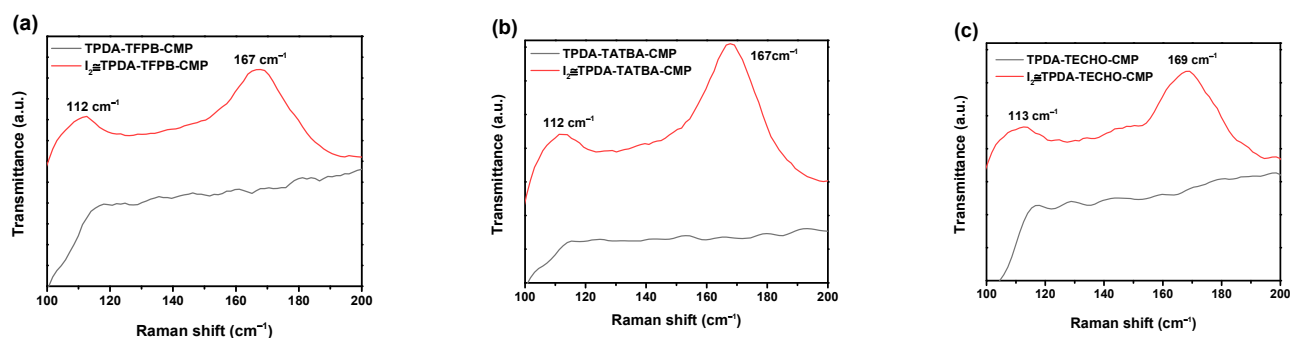


Figure 8. Effects of adsorbed iodine on the Raman spectra of TPDA–TFPB CMP (a), TPDA–TATBA CMP (b), and TPDA–TECHO CMP (c).

3. Experimental Section

Materials. Solvents were purchased from Tansoole and used without any purification. The organic monomers N1,N1'-(1,4-phenylene)bis(N1-(4-aminophenyl)benzene-1,4-diamine) (TPDA) and 4,4',4''-(1,3,5-benzenetriyltri-2,1-ethynediyl)tris[benzaldehyde] (TECHO) were purchased from Bide Pharmatech Ltd., Shanghai, China, while 1,3,5-tris(4-formylphenyl)benzene (TFPB) and 4,4',4''-(1,3,5-triazine-2,4,6-triyl)tris[benzaldehyde] (TATBA) were synthesized according to documented procedures [46,90].

Synthesis of TPDA–TFPB CMP. To a 5 mL Pyrex tube was added TPDA (12.8 mg, 0.027 mmol), TFPB (15.6 mg, 0.04 mmol), and a mixture of o-dichlorobenzene (0.5 mL) and n-butanol (0.5 mL). This was followed by exposure to ultrasound for 15 min. After that, 0.1 mL acetic acid (9 M) was added to the tube, which was then flash-frozen through liquid nitrogen and degassed via five freeze–pump–thaw cycles. The tube was sealed with a flame and then heated at 120 °C for 3 days. After the reaction was complete, the resultant precipitate was immersed in dried DMF for 2 days and further purified by Soxhlet extraction with anhydrous tetrahydrofuran/DMF (1:2, *v/v*) for 2 days. The solid was dried under vacuum at 120 °C to give yellow TPDA–TFPB CMP (80% yield). Elemental analysis (%) of TPDA–TFPB CMP was conducted. We expected C, 86.06; H, 4.81; N 9.12 and found C, 81.87; H, 5.01; N 9.63.

Synthesis of TPDA–TATBA CMP. To a 5 mL Pyrex tube was added TPDA (12.8 mg, 0.027 mmol), TATBA (14.2 mg, 0.036 mmol), and a mixture of o-dichlorobenzene (0.5 mL) and n-butanol (0.5 mL). This was followed by exposure to ultrasound for 15 min. After that, 0.2 mL acetic acid (6 M) was added to the tube, which was then flash-frozen through liquid nitrogen and degassed via five freeze–pump–thaw cycles. The tube was sealed with a flame and then heated at 120 °C for 3 days. After the reaction was complete, the resultant precipitate was immersed in dried DMF for 2 days and further purified by Soxhlet extraction with anhydrous tetrahydrofuran/DMF (1:2, *v/v*) for 2 days. The solid was dried under vacuum at 120 °C to give a red TPDA–TATBA CMP (81% yield). Elemental analysis (%) of TPDA–TATBA CMP was conducted. We expected C, 80.51; H, 4.33; N 15.15 and found C, 75.66; H, 4.49; N 14.56.

Synthesis of TPDA–TECHO CMP. The procedure for synthesizing TPDA–TECHO CMP was similar to that of TPDA–TATBA CMP, but with TPDA (12.8 mg, 0.027 mmol) and TECHO (16.7 mg, 0.036 mmol) used as organic monomers instead. This approach gave a yellowish-red powder (83% yield). Elemental analysis (%) of TPDA–TECHO CMP was conducted. We expected C, 87.38; H, 4.36; N 8.26 and found C, 83.06; H, 4.53; N 8.16.

4. Methods

Fourier transform infrared (FT-IR) spectra were recorded with a Jasco FT/IR-6800 spectrometer (Japan) in the range of 4000–400 cm^{-1} . The spectral signals are presented in wavenumbers (cm^{-1}). The Powder X-ray diffraction (PXRD) patterns were collected on a Rigaku X-ray diffractometer (MiniFlex600) using $\text{Cu-K}\alpha$ radiation ($\lambda = 1.542 \text{ \AA}$). The patterns were recorded in the 2θ range from 2° to 30° with a step size of 0.02° and exposure time of $10^\circ \text{ min}^{-1}$. The porous nature of the samples was determined by N_2 adsorption/desorption isotherms at 77 K using Quantachrome Autosorb-iQ (Shanghai, China). Before testing, the samples were dried under vacuum for 12 h at 120°C . Pore size distribution was calculated using nitrogen adsorption data based on the nonlocal density functional theory (NLDFT) approach. Thermogravimetric analyses (TGA) were carried out on a Thermobalance TGA Q600 thermal gravimetric analyzer under a nitrogen atmosphere. The samples were heated at a rate of $10^\circ\text{C min}^{-1}$ from room temperature to 700°C . Field-emission scanning electron microscopy (FE-SEM) measurements were performed on a Hitachi Regulus8100. Ultraviolet visible infrared spectrophotometer (UV-vis) spectra were recorded with a Jasco V-770 spectrophotometer in the range of 200–700 nm. ^1H NMR and ^{13}C NMR spectra were recorded on a 400 M NMR spectrometer (Bruker AVANCE NEO 400 MHz NMR spectrometer). ^{13}C cross-polarization magic-angle spinning nuclear magnetic resonance (^{13}C CP/MAS NMR) spectroscopy was recorded on Bruker AVANCE III spectrometer (600 MHz). Raman spectrum was recorded on an InVia Qontor spectrometer with an excitation wavelength of 532 nm at room temperature.

5. Conclusions

In summary, three novel conjugated microporous polymers (CMPs) were designed and synthesized under the guidance of topology. A planar rectangular 4-connected organic monomer (TPDA) was used to construct preferred three-dimensional (3D) networks with triangular 3-connected organic monomers (TFPB, TATBA, and TECHO) to produce TPDA–TFPB CMP, TPDA–TATBA CMP, and TPDA–TECHO CMP. The high porosity, good thermostability, uniform micromorphology, and π -conjugated structures of the CMPs encouraged us to investigate their iodine adsorption behaviors. The resultant CMPs exhibited ultrahigh iodine adsorption capacities of 6.48, 6.25, and 6.37 g g^{-1} , respectively, at 348 K and ambient pressure. FT-IR and Raman spectra were used to analyze the adsorption mechanism of iodine. The strong chemical adsorption between the iodine and the imine/tertiary ammonia of the CMPs may contribute to the ultrahigh iodine adsorption capacities. In addition, the 3D network structures with accessible hierarchical pores, uniform micromorphology, and high-density Lewis-base sites (imine and tertiary ammonia of TPDA) could also synergistically lead to their excellent iodine adsorption performance. This research gives guidance for the design of novel CMPs to cope with nuclear pollution in the field of nuclear power.

Supplementary Materials: The following supporting information can be downloaded at: <https://www.mdpi.com/article/10.3390/molecules29102242/s1>, Figure S1. The possible 3D topological structures through the combination of 4-connected and 3-connected monomers; Figure S2. ^1H NMR spectrum of TFPB; Figure S3. ^1H NMR spectrum of TAPBA; Figure S4. ^{13}C CP/MAS NMR spectra of TPDA–TFPB–CMP, TPDA–TATBA–CMP, and TPDA–TECHO–CMP; Figure S5. TGA curves of TPDA–TFPB–CMP and $\text{I}_2 \cong \text{TPDA–TFPB–CMP}$ (a), TPDA–TATBA–CMP and $\text{I}_2 \cong \text{TPDA–TATBA–CMP}$ (b), and TPDA–TECHO–CMP and $\text{I}_2 \cong \text{TPDA–TECHO–CMP}$ (c); Figure S6. The color change of TPDA–TFPB–CMP (left), TPDA–TATBA–CMP (middle), and TPDA–TECHO–CMP (right) before and after I_2 adsorption; Figure S7. PXRD patterns of TPDA–TFPB–CMP and $\text{I}_2 \cong \text{TPDA–TFPB–CMP}$ (a) TPDA–TATBA–CMP and $\text{I}_2 \cong \text{TPDA–TATBA–CMP}$ (b), and TPDA–TECHO–CMP and $\text{I}_2 \cong \text{TPDA–TECHO–CMP}$ (c); Table S1. Comparison of representatively reported adsorbents with our work for iodine vapor adsorption under atmospheric pressure; Figure S8. UV-vis spectra of n-hexane standard solutions of iodine with different concentration (a) and the corresponding calibration curve of absorbance versus iodine concentration established from UV-vis spectra (b) as shown in (a); Figure S9. The I_2 adsorption behavior of the CMPs in n-hexane. The concentration of iodine in n-hexane solution is 100 mg L^{-1} ,

300 mg L⁻¹, and 500 mg L⁻¹, respectively; Figure S10. UV-vis spectra of methanol standard solutions of iodine with different concentration (a) and the corresponding calibration curve of absorbance versus iodine concentration established from UV-vis spectra (b) as shown in (a); Figure S11. Recyclability of TPDA-TFPB-CMP, TPDA-TATBA-CMP, and TPDA-TECHO-CMP in iodine uptake.

Author Contributions: Conceptualization, C.L.; methodology, C.L. and Q.Y.; software, H.H.; resources, Y.G. and X.S.; writing—original draft preparation, C.L.; writing—review and editing, Y.G.; supervision, Y.G.; project administration, Y.G.; funding acquisition, Y.G. and X.S.; S.W., X.S., H.X., S.X. and S.L. conceived the idea and designed the experiment. The manuscript was written with contributions from all authors. All authors have read and agreed to the published version of the manuscript.

Funding: This research was funded the Major Science and Technology Plan of Hainan Province, China (ZDKJ202016), the National Natural Science Foundation of China (22105053 and 22165009), the Key Research and Development Project of Hainan Province (ZDYF2024GXJS005), and the Natural Science Foundation of Hainan Province, China (521QN209).

Institutional Review Board Statement: Not applicable.

Informed Consent Statement: Not applicable.

Data Availability Statement: The authors confirm that most of the data supporting the findings of this study are available within the article and its Supplementary Materials. Raw data are available from the corresponding author (Y.G.) on request.

Acknowledgments: The authors thank Duncan W. Bruce, the University of York, UK, for his valuable discussions on this work.

Conflicts of Interest: The authors declare no competing financial interest.

References

1. Shen, N.; Yang, Z.; Liu, S.; Dai, X.; Xiao, C.; Taylor-Pashow, K.; Li, D.; Yang, C.; Li, J.; Zhang, Y.; et al. ⁹⁹TcO₄⁻ removal from legacy defense nuclear waste by an alkaline-stable 2D cationic metal organic framework. *Nat. Commun.* **2020**, *11*, 5571. [[CrossRef](#)] [[PubMed](#)]
2. Xiong, S.; Tao, J.; Wang, Y.; Tang, J.; Liu, C.; Liu, Q.; Wang, Y.; Yu, G.; Pan, C. Uniform poly(phosphazene-triazine) porous microspheres for highly efficient iodine removal. *Chem. Commun.* **2018**, *54*, 8450–8453. [[CrossRef](#)]
3. Yan, Z.; Yuan, Y.; Tian, Y.; Zhang, D.; Zhu, G. Highly efficient enrichment of volatile iodine by charged porous aromatic frameworks with three sorption sites. *Angew Chem. Int. Ed.* **2015**, *54*, 12733–12737. [[CrossRef](#)] [[PubMed](#)]
4. Zhang, X.; Maddock, J.; Nenoff, T.M.; Denecke, M.A.; Yang, S.; Schröder, M. Adsorption of iodine in metal–organic framework materials. *Chem. Soc. Rev.* **2022**, *51*, 3243–3262. [[CrossRef](#)] [[PubMed](#)]
5. Wang, P.; Xu, Q.; Li, Z.; Jiang, W.; Jiang, Q.; Jiang, D. Exceptional Iodine Capture in 2D Covalent Organic Frameworks. *Adv. Mater.* **2018**, *30*, 1801991. [[CrossRef](#)] [[PubMed](#)]
6. Mushkacheva, G.; Rabinovich, E.; Privalov, V.; Povolotskaya, S.; Shorokhova, V.; Sokolova, S.; Turdakova, V.; Ryzhova, E.; Hall, P.; Schneider, A.B. Thyroid Abnormalities Associated with Protracted Childhood Exposure to ¹³¹I from Atmospheric Emissions from the Mayak Weapons Facility in Russia. *Radiat. Res.* **2006**, *166*, 715–722. [[CrossRef](#)] [[PubMed](#)]
7. Chapman, K.W.; Chupas, P.J.; Nenoff, T.M. Radioactive iodine capture in silver-containing mordenites through nanoscale silver iodide formation. *J. Am. Chem. Soc.* **2010**, *132*, 8897–8899. [[CrossRef](#)] [[PubMed](#)]
8. Pham, T.C.T.; Docao, H.; Hwang, S.I.C.; Song, M.; Choi, D.Y.; Moon, D.; Oleynikov, P.; Yoon, K.B. Capture of Iodine and Organic Iodides using Silica Zeolites and the Semiconductor Behaviour of Iodine in a Silica Zeolite. *Energy Environ. Sci.* **2016**, *9*, 1050–1062. [[CrossRef](#)]
9. Sun, H.; Yang, B.; Li, A. Biomass derived Porous Carbon for Efficient Capture of Carbon Dioxide, Organic Contaminants and Volatile Iodine with Exceptionally High Uptake. *Chem. Eng. J.* **2019**, *372*, 65–73. [[CrossRef](#)]
10. Hu, Y.; Chen, X.; Liu, Z.; Wang, G.; Liao, S. Activated carbon doped with biogenic manganese oxides for the removal of indigo carmine. *J. Environ. Manag.* **2015**, *166*, 512–518. [[CrossRef](#)]
11. Al-Mamoori, A.; Alsabokh, M.; Lawson, S.; Rownaghi, A.A.; Rezaei, F. Development of Bismuth-mordenite Adsorbents for Iodine Capture from Off-gas Streams. *Chem. Eng. J.* **2020**, *391*, 123583. [[CrossRef](#)]
12. Guan, Y.; Li, Y.; Zhou, J.; Zhang, T.; Ding, J.; Xie, Z.; Wang, L. Defect Engineering of Nanoscale Hf-Based Metal–Organic Frameworks for Highly Efficient Iodine Capture. *Inorg. Chem.* **2021**, *60*, 9848–9856. [[CrossRef](#)] [[PubMed](#)]
13. Zeng, M.; Wang, Q.; Tan, Y.; Hu, S.; Zhao, H.; Long, L.; Kurmoo, M. Rigid Pillars and Double Walls in a Porous Metal–Organic Framework: Single-Crystal to Single-Crystal, Controlled Uptake and Release of Iodine and Electrical Conductivity. *J. Am. Chem. Soc.* **2010**, *132*, 2561–2563. [[CrossRef](#)] [[PubMed](#)]

14. Yu, R.; Li, Q.; Li, Z.; Wang, X.; Xia, L. Analysis of Radioactive Iodine Trapping Mechanism by Zinc-Based Metal–Organic Frameworks with Various N-Containing Carboxylate Ligands. *ACS Appl. Mater. Interfaces* **2023**, *15*, 35082–35091. [[CrossRef](#)] [[PubMed](#)]
15. Bennett, T.D.; Saines, P.J.; Keen, D.A.; Tan, J.; Cheetham, A.K. Ball-milling-induced amorphization of zeolitic imidazolate frameworks (ZIFs) for the irreversible trapping of iodine. *Chem. Eur. J.* **2013**, *19*, 7049–7055. [[CrossRef](#)] [[PubMed](#)]
16. Wen, Z.; Wang, S.; Fu, S.; Qian, J.; Xu, H.; Zuo, K.; Su, X.; Zeng, C.; Gao, Y. A Two-dimensional Dual-pore Covalent Organic Framework for Efficient Iodine Capture. *Chem. Res. Chinese U.* **2022**, *38*, 472–477. [[CrossRef](#)]
17. Chang, J.; Li, H.; Zhao, J.; Guan, X.; Li, C.; Yu, G.; Valtchev, V.; Yan, Y.; Qiu, S.; Fang, Q. Tetrathiafulvalene-based covalent organic frameworks for ultrahigh iodine capture. *Chem. Sci.* **2021**, *12*, 8452–8457. [[CrossRef](#)] [[PubMed](#)]
18. Guo, X.; Li, Y.; Zhang, M.; Cao, K.; Tian, Y.; Qi, Y.; Li, S.; Li, K.; Yu, X.; Ma, L. Colyliform Crystalline 2D Covalent Organic Frameworks (COFs) with Quasi-3D Topologies for Rapid I₂ Adsorption. *Angew. Chem. Int. Ed.* **2020**, *59*, 22697–22705. [[CrossRef](#)] [[PubMed](#)]
19. Yan, X.; Yang, Y.; Li, G.; Zhang, J.; He, Y.; Wang, R.; Lin, Z.; Cai, Z. Thiophene-based covalent organic frameworks for highly efficient iodine capture. *Chin. Chem. Lett.* **2023**, *34*, 107201. [[CrossRef](#)]
20. Liu, C.; Jin, Y.; Yu, Z.; Gong, L.; Wang, H.; Yu, B.; Zhang, W.; Jiang, J. Transformation of Porous Organic Cages and Covalent Organic Frameworks with Efficient Iodine Vapor Capture Performance. *J. Am. Chem. Soc.* **2022**, *144*, 12390–12399. [[CrossRef](#)]
21. Luo, S.; Yan, Q.; Wang, S.; Hu, H.; Xiao, S.; Su, X.; Xu, H.; Gao, Y. Conjugated Microporous Polymers Based on Octet and Tetratopic Linkers for Efficient Iodine Capture. *ACS Appl. Mater. Interfaces* **2023**, *15*, 46408–46416. [[CrossRef](#)] [[PubMed](#)]
22. Xu, M.; He, Q.; Chen, F.; Zhao, Z.; Wang, Z.; Hua, D. Thermal-Responsive Conjugated Micropore Polymers for Smart Capture of Volatile Iodine. *ACS Appl. Mater. Interfaces* **2023**, *15*, 31421–31429. [[CrossRef](#)]
23. Zuo, H.; Lu, W.; Zhang, W.; Li, Y.; Liao, Y. High-Yield Synthesis of Pyridyl Conjugated Microporous Polymer Networks with Large Surface Areas: From Molecular Iodine Capture to Metal-Free Heterogeneous Catalysis. *Macromol. Rapid Commun.* **2020**, *41*, 2000489. [[CrossRef](#)]
24. Sigen, A.; Zhang, Y.; Li, Z.; Xia, H.; Xue, M.; Liu, X.; Mu, Y. Highly efficient and reversible iodine capture using a metalloporphyrin-based conjugated microporous polymer. *Chem. Commun.* **2014**, *50*, 8495–8498.
25. Yan, Z.; Qiao, Y.; Wang, J.; Xie, J.; Cui, B.; Fu, Y.; Lu, J.; Yang, Y.; Bu, N.; Yuan, Y. An Azo-Group-Functionalized Porous Aromatic Framework for Achieving Highly Efficient Capture of Iodine. *Molecules* **2022**, *27*, 6297. [[CrossRef](#)]
26. Wang, J.; Wang, C.; Wang, H.; Jin, B.; Zhang, P.; Li, L.; Miao, S. Synthesis of N-containing porous aromatic frameworks via Scholl reaction for reversible iodine capture. *Micropor. Mesopor. Mater.* **2021**, *310*, 110596. [[CrossRef](#)]
27. Xia, L.; Yang, D.; Zhang, H.; Zhang, Q.; Bu, N.; Song, P.; Yan, Z.; Yuan, Y. Constructing “breathing” dynamic skeletons with extra π -conjugated adsorption sites for iodine capture. *RSC Adv.* **2019**, *9*, 20852–20856. [[CrossRef](#)]
28. Pei, C.; Ben, T.; Xu, S.; Qiu, S. Ultrahigh iodine adsorption in porous organic frameworks. *J. Mater. Chem. A* **2014**, *2*, 7179–7187. [[CrossRef](#)]
29. Wang, J.; Wang, X.; Deng, Y.; Wu, T.; Chen, J.; Liu, J.; Xu, L.; Zang, Y. Preparation of an electron-rich polyimide-based hypercrosslinked polymer for high-efficiency and reversible iodine capture. *Polymer* **2023**, *267*, 125665. [[CrossRef](#)]
30. Samanta, P.; Dutta, S.; Let, S.; Sen, A.; Shirolkar, M.M.; Ghosh, S.K. Hydroxy-Functionalized Hypercrosslinked Polymers (HCPs) as Dual Phase Radioactive Iodine Scavengers: Synergy of Porosity and Functionality. *ChemPlusChem* **2022**, *87*, e202200212. [[CrossRef](#)]
31. Luo, S.; Zeng, Z.; Wang, H.; Xiong, W.; Song, B.; Zhou, C.; Duan, A.; Tan, X.; He, Q.; Zeng, G. Recent progress in conjugated microporous polymers for clean energy: Synthesis, modification, computer simulations, and applications. *Prog. Polym. Sci.* **2021**, *115*, 101374.
32. Tian, Y.; Zhu, G. Porous Aromatic Frameworks (PAFs). Porous aromatic frameworks (PAFs). *Chem. Rev.* **2020**, *120*, 8934–8986. [[CrossRef](#)]
33. Xu, Y.; Jin, S.; Xu, H.; Nagai, A.; Jiang, D. Conjugated microporous polymers: Design, synthesis and application. *Chem. Soc. Rev.* **2013**, *42*, 8012–8031. [[CrossRef](#)] [[PubMed](#)]
34. Ren, H.; Ben, T.; Sun, F.; Guo, M.; Jing, X.; Ma, H.; Cai, K.; Qiu, S.; Zhu, G. Synthesis of a porous aromatic framework for adsorbing organic pollutants application. *J. Mater. Chem.* **2011**, *21*, 10348–10353. [[CrossRef](#)]
35. Zhao, H.; Jin, Z.; Su, H.; Jing, X.; Sun, F.; Zhu, G. Targeted synthesis of a 2D ordered porous organic framework for drug release. *Chem. Commun.* **2011**, *47*, 6389–6391. [[CrossRef](#)] [[PubMed](#)]
36. Ben, T.; Ren, H.; Ma, S.; Cao, D.; Lan, J.; Jing, X.; Wang, W.; Xu, J.; Deng, F.; Simmons, J.M. Targeted Synthesis of a Porous Aromatic Framework with High Stability and Exceptionally High Surface Area. *Angew. Chem. Int. Ed.* **2009**, *48*, 9457–9460. [[CrossRef](#)]
37. Zou, X.; Ren, H.; Zhu, G. Topology-directed design of porous organic frameworks and their advanced applications. *Chem. Commun.* **2013**, *49*, 3925–3936. [[CrossRef](#)]
38. Modak, A.; Nandi, M.; Mondal, J.; Bhaumik, A. Porphyrin based porous organic polymers: Novel synthetic strategy and exceptionally high CO₂ adsorption capacity. *Chem. Commun.* **2012**, *48*, 248–250. [[CrossRef](#)] [[PubMed](#)]
39. Yuan, Y.; Ren, H.; Sun, F.; Jing, X.; Cai, K.; Zhao, X.; Wang, Y.; Wei, Y.; Zhu, G. Sensitive detection of hazardous explosives via highly fluorescent crystalline porous aromatic frameworks. *J. Mater. Chem.* **2012**, *22*, 24558. [[CrossRef](#)]

40. Yuan, Y.; Ren, H.; Sun, F.; Jing, X.; Cai, K.; Zhao, X.; Wang, Y.; Wei, Y.; Zhu, G. Targeted Synthesis of a 3D Crystalline Porous Aromatic Framework with Luminescence Quenching Ability for Hazardous and Explosive Molecules. *J. Phys. Chem. C* **2012**, *116*, 26431–26435. [\[CrossRef\]](#)
41. Song, S.; Shi, Y.; Liu, N.; Liu, F. Theoretical Screening and Experimental Synthesis of Ultrahigh-Iodine Capture Covalent Organic Frameworks. *ACS Appl. Mater. Interfaces* **2021**, *13*, 10513–10523. [\[CrossRef\]](#) [\[PubMed\]](#)
42. Yin, Z.; Xu, S.; Zhan, T.; Qi, Q.; Wu, Z.; Zhao, X. Ultrahigh Volatile Iodine Uptake by Hollow Microspheres Formed from a Heteropore Covalent Organic Framework. *Chem. Commun.* **2017**, *53*, 7266–7269. [\[CrossRef\]](#) [\[PubMed\]](#)
43. Wang, C.; Wang, Y.; Ge, R.; Song, X.; Xing, X.; Jiang, Q.; Lu, H.; Hao, C.; Guo, X.; Gao, Y. A 3D Covalent Organic Framework with Exceptionally High Iodine Capture Capability. *Chem. Eur. J.* **2018**, *24*, 585–589. [\[CrossRef\]](#) [\[PubMed\]](#)
44. Ren, F.; Zhu, Z.; Qian, X.; Liang, W.; Mu, P.; Sun, H.; Liu, J.; Li, A. Novel Thiophene-bearing Conjugated Microporous Polymer Honeycomb-like Porous Spheres with Ultrahigh Iodine Uptake. *Chem. Commun.* **2016**, *52*, 9797–9800. [\[CrossRef\]](#) [\[PubMed\]](#)
45. Hu, X.; Wang, H.; Faul, C.F.J.; Wen, J.; Wei, Y.; Zhu, M.; Liao, Y. Crosslinking Alkylation Strategy to Construct Nitrogen-enriched Tetraphenylmethane-based Porous Organic Polymers as Efficient Carbon Dioxide and Iodine Adsorbents. *Chem. Eng. J.* **2020**, *382*, 122998. [\[CrossRef\]](#)
46. Grunenberg, L.; Savasci, G.; Terban, M.W.; Duppel, V.; Etter, I.M.M.; Dinnebier, R.E.; Ochsenfeld, C.; Lotsch, B.V. Amine-Linked Covalent Organic Frameworks as a Platform for Postsynthetic Structure Interconversion and Pore-Wall Modification. *J. Am. Chem. Soc.* **2021**, *143*, 3430–3438. [\[CrossRef\]](#) [\[PubMed\]](#)
47. Wang, N.; Feng, L.; Xu, X.; Feng, S. Dynamic covalent bond cross-linked luminescent silicone elastomer with self-healing and recyclable properties. *Macromol. Rapid Commun.* **2022**, *43*, e2100885. [\[CrossRef\]](#) [\[PubMed\]](#)
48. Xie, Y.; Pan, T.; Lei, Q.; Chen, C.; Dong, X.; Yuan, Y.; Shen, J.; Cai, Y.; Zhou, C.; Pinnau, I.; et al. Ionic Functionalization of Multivariate Covalent Organic Frameworks to Achieve an Exceptionally High Iodine-Capture Capacity. *Angew. Chem. Int. Ed.* **2021**, *60*, 22432–22440. [\[CrossRef\]](#)
49. Li, J.; Zhang, H.; Zhang, L.; Wang, K.; Wang, Z.; Liu, G.; Zhao, Y.; Zeng, Y. Two-dimensional covalent–organic frameworks for ultrahigh iodine capture. *J. Mater. Chem. A* **2020**, *8*, 9523–9527. [\[CrossRef\]](#)
50. Guo, X.; Tian, Y.; Zhang, M.; Li, Y.; Wen, R.; Li, X.; Li, X.; Xue, Y.; Ma, L.; Xia, C.; et al. Mechanistic insight into hydrogen-bond-controlled crystallinity and adsorption property of covalent organic frameworks from flexible building blocks. *Chem. Mater.* **2018**, *30*, 2299–2308. [\[CrossRef\]](#)
51. Geng, T.; Ye, S.; Zhu, Z.; Zhang, W. Triazine-based conjugated microporous polymers with *N,N,N',N'*-tetraphenyl-1,4-phenylenediamine, 1,3,5-tris(diphenylamino)benzene and 1,3,5-tris[(3-methylphenyl)-phenylamino]benzene as the core for high iodine capture and fluorescence sensing of *o*-nitrophenol. *J. Mater. Chem. A* **2018**, *6*, 2808–2816.
52. Guo, Z.; Sun, P.; Zhang, X.; Lin, J.; Shi, T.; Liu, S.; Sun, A.; Li, Z. Amorphous porous organic polymers based on schiff-base chemistry for highly efficient iodine capture. *Chem. Asian J.* **2018**, *13*, 2046–2053. [\[CrossRef\]](#) [\[PubMed\]](#)
53. Tian, P.; Ai, Z.; Hu, H.; Wang, M.; Li, Y.; Gao, X.; Qian, J.; Su, X.; Xiao, S.; Xu, H.; et al. Synthesis of Electron-Rich Porous Organic Polymers via Schiff-Base Chemistry for Efficient Iodine Capture. *Molecules* **2022**, *27*, 5161. [\[CrossRef\]](#) [\[PubMed\]](#)
54. Qian, X.; Wang, B.; Zhu, Z.; Sun, H.; Ren, F.; Mu, P.; Ma, C.; Liang, W.; Li, A. Novel N-rich Porous Organic Polymers with Extremely High Uptake for Capture and Reversible Storage of Volatile Iodine. *J. Hazard. Mater.* **2017**, *338*, 224–232. [\[CrossRef\]](#) [\[PubMed\]](#)
55. Su, K.; Wang, W.; Li, B.; Yuan, D. Azo-Bridged Calix[4]resorcinarene-Based Porous Organic Frameworks with Highly Efficient Enrichment of Volatile Iodine. *ACS Sustain. Chem. Eng.* **2018**, *6*, 17402–17409. [\[CrossRef\]](#)
56. An, S.; Zhu, X.; He, Y.; Yang, L.; Wang, H.; Jin, S.; Hu, J.; Liu, H. Porosity modulation in two-dimensional covalent organic frameworks leads to enhanced iodine adsorption performance. *Ind. Eng. Chem. Res.* **2019**, *58*, 10495–10502. [\[CrossRef\]](#)
57. Jiang, Q.; Huang, H.; Tang, Y.; Zhang, Y.; Zhong, C. Highly porous covalent triazine frameworks for reversible iodine capture and efficient removal of dye. *Ind. Eng. Chem. Res.* **2018**, *57*, 15114–15121. [\[CrossRef\]](#)
58. Sun, H.; La, P.; Zhu, Z.; Liang, W.; Yang, B.; Li, A. Capture and reversible storage of volatile iodine by porous carbon with high capacity. *J. Mater. Sci.* **2015**, *50*, 7326–7332. [\[CrossRef\]](#)
59. Liao, Y.; Weber, J.; Mills, B.M.; Ren, Z.; Faul, C.F.J. Highly efficient and reversible iodine capture in hexaphenylbenzene-based conjugated microporous polymers. *Macromolecules* **2016**, *49*, 6322–6333. [\[CrossRef\]](#)
60. Qi, B.; Liu, Y.; Zheng, T.; Gao, Q.; Yan, X.; Jiao, Y.; Yang, Y. Highly efficient capture of iodine by Cu/MIL-101. *J. Solid State Chem.* **2018**, *258*, 49–55. [\[CrossRef\]](#)
61. Li, H.; Ding, X.; Han, B. Porous azo-bridged porphyrin–phthalocyanine network with high iodine capture capability. *Chem. Eur. J.* **2016**, *22*, 11863–11868. [\[CrossRef\]](#) [\[PubMed\]](#)
62. Ren, Y.; Zhang, W.; Zhu, Y.; Wang, D.; Yu, G.; Kuang, G. Nitrogen-rich porous polyaminal network as a platform for iodine adsorption through physical and chemical interaction. *J. Appl. Polym. Sci.* **2018**, *135*, 46106. [\[CrossRef\]](#)
63. Riley, B.J.; Chun, J.; Ryan, J.V.; Matyas, J.; Li, X.; Matson, D.W.; Sundaram, S.K.; Strachan, D.M.; Vienna, J.D. Chalcogen-based aerogels as a multifunctional platform for remediation of radioactive iodine. *RSC Adv.* **2011**, *1*, 1704–1715. [\[CrossRef\]](#)
64. Dang, Q.; Wang, X.; Zhan, Y.; Zhang, X. An azo-linked porous triptycene network as an absorbent for CO₂ and iodine uptake. *Polymer Chem.* **2016**, *7*, 643–647. [\[CrossRef\]](#)
65. Li, Y.; Chen, W.; Hao, W.; Li, Y.; Chen, L. Covalent organic frameworks constructed from flexible building blocks with high adsorption capacity for pollutants. *ACS Appl. Nano Mater.* **2018**, *1*, 4756–4761. [\[CrossRef\]](#)

66. Subrahmanyam, K.S.; Sarma, D.; Malliakas, C.D.; Polychronopoulou, K.; Riley, B.J.; Pierce, D.A.; Chun, J.; Kanatzidis, M.G. Chalcogenide aerogels as sorbents for radioactive iodine. *Chem. Mater.* **2015**, *27*, 2619–2626. [\[CrossRef\]](#)
67. Zhu, Y.; Ji, Y.; Wang, D.; Zhang, Y.; Tang, H.; Jia, X.; Song, M.; Yu, G.; Kuang, G. BODIPY-based conjugated porous polymers for highly efficient volatile iodine capture. *J. Mater. Chem. A* **2017**, *5*, 6622–6629. [\[CrossRef\]](#)
68. Qian, X.; Zhu, Z.; Sun, H.; Ren, F.; Mu, P.; Chen, L.; Li, A. Capture and Reversible Storage of Volatile Iodine by Novel Conjugated Microporous Polymers Containing Thiophene Units. *ACS Appl. Mater. Interfaces* **2016**, *8*, 21063–21069. [\[CrossRef\]](#) [\[PubMed\]](#)
69. Chen, P.; He, X.; Pang, M.; Dong, X.; Zhao, S.; Zhang, W. Iodine capture using Zr-based metal–organic frameworks (Zr-MOFs): Adsorption performance and mechanism. *ACS Appl. Mater. Interfaces* **2020**, *12*, 20429–20439. [\[CrossRef\]](#)
70. Chen, Y.; Sun, H.; Yang, R.; Wang, T.; Pei, C.; Xiang, Z.; Zhu, Z.; Liang, W.; Li, A.; Deng, W. Synthesis of conjugated microporous polymer nanotubes with large surface areas as absorbents for iodine and CO₂ uptake. *J. Mater. Chem. A* **2015**, *3*, 87–91. [\[CrossRef\]](#)
71. Ma, H.; Chen, J.; Tan, L.; Bu, J.; Zhu, Y.; Tan, B.; Zhang, C. Nitrogen-Rich Triptycene-Based Porous Polymer for Gas Storage and Iodine Enrichment. *ACS Macro Lett.* **2016**, *5*, 1039–1043. [\[CrossRef\]](#) [\[PubMed\]](#)
72. Sava, D.F.; Chapman, K.W.; Rodriguez, M.A.; Greathouse, J.A.; Crozier, P.S.; Zhao, H.; Chupas, P.J.; Nenoff, T.M. Competitive I₂ Sorption by Cu-BTC from Humid Gas Streams. *Chem. Mater.* **2013**, *25*, 2591–2596. [\[CrossRef\]](#)
73. Sava, D.F.; Rodriguez, M.A.; Chapman, K.W.; Chupas, P.J.; Greathouse, J.A.; Crozier, P.S.; Nenoff, T.M. Capture of volatile iodine, a gaseous fission product, by zeolitic imidazolate framework-8. *J. Am. Chem. Soc.* **2011**, *133*, 12398–12401. [\[CrossRef\]](#) [\[PubMed\]](#)
74. Mehlana, G.; Ramon, G.; Bourne, S.A. A 4-fold interpenetrated diamondoid metal-organic framework with large channels exhibiting solvent sorption properties and high iodine capture. *Microporous Mesoporous Mater.* **2016**, *231*, 21–30. [\[CrossRef\]](#)
75. Park, K.C.; Cho, J.; Lee, C.Y. Porphyrin and pyrene-based conjugated microporous polymer for efficient sequestration of CO₂ and iodine and photosensitization for singlet oxygen generation. *RSC Adv.* **2016**, *6*, 75478–75481. [\[CrossRef\]](#)
76. Mu, P.; Sun, H.; Chen, T.; Zhang, W.; Zhu, Z.; Liang, W.; Li, A. A Sponge-Like 3D-PPy Monolithic Material for Reversible Adsorption of Radioactive Iodine. *Macromol. Mater. Eng.* **2017**, *302*, 1700156. [\[CrossRef\]](#)
77. Li, L.; Chen, R.; Li, Y.; Xiong, T.; Li, Y. Novel cotton fiber-covalent organic framework hybrid monolith for reversible capture of iodine. *Cellulose* **2020**, *27*, 5879–5892. [\[CrossRef\]](#)
78. Sava, D.F.; Garino, T.J.; Nenoff, T.M. Iodine confinement into metal–organic frameworks (MOFs): Low-temperature sintering glasses to form novel glass composite material (GCM) alternative waste forms. *Ind. Eng. Chem. Res.* **2012**, *51*, 614–620. [\[CrossRef\]](#)
79. Wang, Y.; Sotzing, G.A.; Weiss, R.A. Sorption of iodine by polyurethane and melamine-formaldehyde foams using iodine sublimation and iodine solutions. *Polymer* **2006**, *47*, 2728–2740. [\[CrossRef\]](#)
80. Liu, Q.; Ma, J.; Dong, Y. Highly efficient iodine species enriching and guest-driven tunable luminescent properties based on a cadmium (II)-triazole MOF. *Chem. Comm.* **2011**, *47*, 7185–7187. [\[CrossRef\]](#)
81. Yin, Z.; Wang, Q.; Zeng, M. Iodine Release and Recovery, Influence of Polyiodide Anions on Electrical Conductivity and Nonlinear Optical Activity in an Interdigitated and Interpenetrated bi Pillared-bilayer Metal-organic Framework. *J. Am. Chem. Soc.* **2012**, *134*, 4857–4863. [\[CrossRef\]](#) [\[PubMed\]](#)
82. Hasell, T.; Schmidtman, M.; Cooper, A.I. Molecular Doping of Porous Organic Cages. *J. Am. Chem. Soc.* **2011**, *133*, 14920–14923. [\[CrossRef\]](#) [\[PubMed\]](#)
83. Wang, Z.; Zhang, Y.; Liu, T.; Kurmoo, M.; Gao, S. [Fe₃(HCOO)₆]: A Permanent Porous Diamond Framework Displaying H₂/N₂ Adsorption, Guest Inclusion, and Guest-Dependent Magnetism. *Adv. Funct. Mater.* **2007**, *17*, 1523–1536. [\[CrossRef\]](#)
84. Riley, B.J.; Chong, S.; Schmid, J.; Marcial, J.; Nienhuis, E.T.; Ber, M.K.; Lee, S.; Canfield, N.L.; Kim, S.; Derewinski, M.A.; et al. Role of Zeolite Structural Properties toward Iodine Capture: A Head-to-head Evaluation of Framework Type and Chemical Composition. *ACS Appl. Mater. Interfaces* **2022**, *14*, 18439–18452. [\[CrossRef\]](#) [\[PubMed\]](#)
85. Katsoulidis, P.; He, J.; Kanatzidis, M.G. Functional monolithic polymeric organic framework aerogel as reducing and hosting media for Ag nanoparticles and application in capturing of iodine vapors. *Chem. Mater.* **2012**, *24*, 1937–1943. [\[CrossRef\]](#)
86. Haefner, D. *Methods of Gas Phase Capture of Iodine from Fuel Reprocessing Off-Gas: A Literature Survey*; Idaho National Laboratory: Idaho Falls, ID, USA, 2007.
87. Abrahams, B.F.; Moylan, M.; Orchard, S.D.; Robson, R. Zinc Saccharate: A Robust, 3D Coordination Network with Two Types of Isolated, Parallel Channels, One Hydrophilic and the Other Hydrophobic. *Angew. Chem. Int. Ed.* **2003**, *42*, 1848–1851. [\[CrossRef\]](#)
88. Kang, X.; Han, X.; Yuan, C.; Cheng, C.; Liu, Y.; Cui, Y. Reticular Synthesis of the Topology Covalent Organic Frameworks. *J. Am. Chem. Soc.* **2020**, *142*, 16346–16356. [\[CrossRef\]](#)
89. Qian, C.; Li, X.; Teo, W.; Gao, Q.; Wei, W. Sub-Stoichiometric Covalent Organic Frameworks. *Adv. Funct. Mater.* **2024**, 2313905. [\[CrossRef\]](#)
90. Lan, Y.; Han, X.; Tong, M.; Huang, H.; Yang, Q.; Liu, D.; Zhao, X.; Zhong, C. Materials genomics methods for high-throughput construction of COFs and targeted synthesis. *Nat. Commun.* **2018**, *9*, 5274.

Disclaimer/Publisher’s Note: The statements, opinions and data contained in all publications are solely those of the individual author(s) and contributor(s) and not of MDPI and/or the editor(s). MDPI and/or the editor(s) disclaim responsibility for any injury to people or property resulting from any ideas, methods, instructions or products referred to in the content.